

Nonlinear Generalized Lifting-Line Coupling Algorithms for Pre/Poststall Flows

S. Gallay* and E. Laurendeau†

École Polytechnique de Montréal, Montréal, Québec H3C 3A7, Canada

DOI: 10.2514/1.J053530

Numerical algorithms and solutions of generalized nonlinear lifting-line theory over an elliptical wing are examined, with emphasis on near/poststall flows. First, a thorough analysis on the circulation-based and angle-of-attack-based correction methods (Γ and α methods, respectively) highlights their respective numerical poststall characteristics. The stability of the method is demonstrated, producing single and multiple solutions in the pre- and poststall regions, respectively. Second, artificial dissipation added to the α method is shown to be an effective means of controlling the poststall flow region. Finally, a strongly coupled algorithm is presented, allowing to bypass the interpolation phase via the use of Legendre polynomials. The model sheds light on poststall flow behavior, in agreement with several papers studying formation of stall cell patterns.

Nomenclature

| | |
|---------------------|---|
| a | = $dcl/d\alpha_e$ slope of the section lift coefficient |
| b | = wingspan, m |
| CL | = $0.5\rho V_\infty^2/S$, wing lift coefficient |
| Cl_{inv} | = $0.5\rho V_\infty^2/c$, inviscid section lift coefficient |
| Cl_{vi} | = $0.5\rho V_\infty^2/c$, viscous section lift coefficient |
| CL_{max} | = $0.5\rho V_\infty^2/S$, maximum lift coefficient |
| Cl_{av} | = slope of the viscous section lift coefficient, rad |
| c | = chord, m |
| V_∞ | = freestream velocity, m/s |
| w_{ind} | = induced downwash velocity, m/s |
| α | = wing angle of attack, rad |
| $\alpha_{CL_{max}}$ | = angle of attack at maximum lift coefficient, rad |
| α_e | = effective angle of attack, rad |
| α_i | = induced angle of attack, rad |
| α_{0l} | = section angle of attack at zero lift, rad |
| Γ | = circulation magnitude, m^2/s |
| η | = constant viscous factor [0,1] simulating linear viscous effects |
| λ | = wing aspect ratio |
| Φ | = sweep angle, rad |
| ϕ | = $\arccos(-y/s)$, spanwise location, Fourier space, rad |
| φ | = section twist angle, rad |

I. Introduction

THIS paper presents developments on aerodynamic analysis over wings using a circulation-based approach coupled to viscous sectional data. The objective is to provide an efficient and robust method for obtaining aerodynamic lift curves in the linear and nonlinear pre/poststall region for various wing planforms with accuracy commensurate with preliminary aircraft design requirements.

The development of rapid aerodynamic models to predict the maximum lift of arbitrary wing planforms has received attention in the literature. One of the most employed methods is that of Valarezo and Chin [1], used in industry at Boeing and Bombardier Aerospace

Presented as Paper 2014-1105 at the 52nd Aerospace Sciences Meeting, National Harbor, MD, 13–17 January 2014; received 7 April 2014; revision received 11 March 2015; accepted for publication 16 March 2015; published online 29 April 2015. Copyright © 2015 by Gallay and Laurendeau. Published by the American Institute of Aeronautics and Astronautics, Inc., with permission. Copies of this paper may be made for personal or internal use, on condition that the copier pay the \$10.00 per-copy fee to the Copyright Clearance Center, Inc., 222 Rosewood Drive, Danvers, MA 01923; include the code 1533-385X/15 and \$10.00 in correspondence with the CCC.

*Ph.D. Candidate, Department of Mechanical Engineering, C.P. 6079, Centre-Ville. Student Member AIAA.

†Assistant Professor, Department of Mechanical Engineering, C.P. 6079, Centre-Ville. Senior Member AIAA.

(see Cebeci et al. [2]). The method uses the panel method [3] to obtain the surface wing pressures and uses a semi-empirical relation to correlate maximum lift with sectional pressure differences evaluated along the span of the wing. Another more recent method is that of Phillips and Alley [4]. The method uses lifting-line theory to evaluate sectional lift properties and correlates these with computational fluid dynamics (CFD) derived correlations by introducing additional coefficients in their analytical expressions. In both works, semi-empirical relations are employed for the correlations; the former uses experimental data to devise a function based on the local Reynolds number and freestream Mach number [1], whereas the latter uses CFD calculations for calibration at a fixed Reynolds number (3 million) and is limited to wings with linear taper and linear twist distributions [4]. Both target the evaluation of CL_{max} and do not aim at estimating poststall behavior.

The present work is examining another class of methods devised to analyze wings of arbitrary shapes and various local Reynolds numbers. These methods provide a means to determine the entire lift curve, encompassing the linear, prestall, and poststall regions. The maximum lift coefficient is therefore implicitly obtained. The focus is on a physics-based reduced-order model, using Prandtl lifting-line theory (LLT). Numerical implementation is performed via the modified LLT proposed by Weissinger [5] and later simplified by Blackwell [6] suitable for the calculation of straight/swept wings with high to moderate aspect ratios. The continuous form of the discretization of Prandtl's theory is sometimes referred as the finite or vortex step method.

Viscous effects are taken into account by introducing corrections to the inviscid model using two-dimensional viscous data, historically obtained through wind-tunnel testing of airfoils [7]. The method is referred to as the nonlinear lifting-line theory, for which two specific implementations exists. The Γ method applies the corrections on the lift circulation Γ [8–10] and suffers from two drawbacks: 1) it requires important underrelaxation to converge, lengthening the solution times, and 2) it has been shown to fail at poststall angles of attacks [11]. The α method has been devised to avoid these difficulties, as shown by Tseng and Lan [12] and van Dam [13]. The method wisely provides the viscous correction through changes in angle of attack.

The encompassing idea behind these inviscid methods is to introduce viscous effects by changing the wing's sectional circulation or angle of attack to match the precise viscous sectional airfoil data, assuming such data already exist in form of a CFD or experimental lift-curve database. Previous works typically use a loosely coupled algorithm to compute the corrections. Here, a strongly coupled procedure is proposed and is shown to outperform the loosely coupled methods in the prestall region by achieving quadratic convergence rates. In the poststall region, the strongly coupled procedure suffers from radius-of-convergence initialization but, once settled, manages to recover near quadratic convergence rates.

The paper is divided as follows. Following a very brief review of the baseline analytical solutions of the flow over an elliptical wing and the potential flow approaches, Sec. IV presents a detailed account of the available viscous-inviscid coupling strategies, namely the angle of attack and circulation-based procedures. The influence of the downwash formulation and the effects on the lift distribution are therein examined. Section V presents a novel strongly coupled procedure and introduces Legendre polynomials. It also presents the use of artificial dissipation to stabilize the angle-of-attack-based procedure, before a final conclusion.

II. Elliptical Wing

For an elliptical wing, the lift of the wing can be analytically described using Prandtl lifting-line theory [14]. In particular, the section lift coefficient at the effective angle of attack is the same as the lift coefficient of the wing, $Cl(\alpha_e) = CL(\alpha)$:

$$\frac{dCL}{d\alpha} = \frac{dCl}{d\alpha_e} \frac{d\alpha_e}{d\alpha} = a \frac{d(\alpha - \alpha_i)}{d\alpha} = a \left(1 - \frac{d\alpha_i}{dCL} \frac{dCL}{d\alpha} \right) \quad (1)$$

where $a = dCl/d\alpha_e$ is the slope of the section lift coefficient. The elliptic wing also generates a downwash angle $\alpha_i = CL/\pi\lambda$, so that the three-dimensional lift curve slope is

$$\frac{dCL}{d\alpha} = \frac{a}{1 + a/\pi\lambda} \quad (2)$$

The lift coefficient can then be calculated for any linear section lift coefficient curve, including a linear viscous one. For example, by taking a hypothetical constant theoretical viscous slope of $a = \eta 2\pi$, the lift coefficient becomes

$$CL(\alpha) = \frac{\eta 2\pi}{1 + 2\eta/\lambda} = \frac{\eta 2\pi\lambda}{\lambda + 2\eta} \quad (3)$$

Equation (3) provides a validation case for Sec. IV once the numerical methods are presented.

III. Vortex Step and Vortex Lattice Methods

Two different implementations of the potential flow theory have been implemented and validated: the vortex step method proposed by Blackwell [6], and the vortex lattice method formulation of Katz and Plotkin [15]. The control points are typically located at the three-quarter-chord line of the panel to ensure a slope of the two-dimensional lift angle-of-attack curve equal to 2π . This is correct for small-angle-of-attack flows where $\sin(\alpha) \approx \alpha$ is valid. The position of the points in the present method has been adapted to ensure a correct slope even for high angles of attack. The two different codes show similar results and agree with the analytical result (Fig. 1) for the case of an elliptical wing with aspect ratio of 12.7. For the remainder of the paper, the vortex step method is used, unless otherwise noted.

IV. Loosely Coupled Algorithms

A. Γ Methods

Different implementations of coupling algorithms have been tested to ensure robustness in the poststall region. Indeed, the methods often show negligible differences for small angles of attack but can encounter problems near prestall and poststall angles. A typical Γ method iterative coupling procedure uses the following steps in a loosely coupled fashion.

1) Assume a lift distribution along the span (i.e., elliptical distribution).

2) Calculate the induced angle of attack for each section y_n using

$$\alpha_i(y_n) = \frac{1}{4\pi V_\infty} \int_{-b/2}^{b/2} \frac{(d\Gamma/dy)dy}{y_n - y} \quad (4)$$

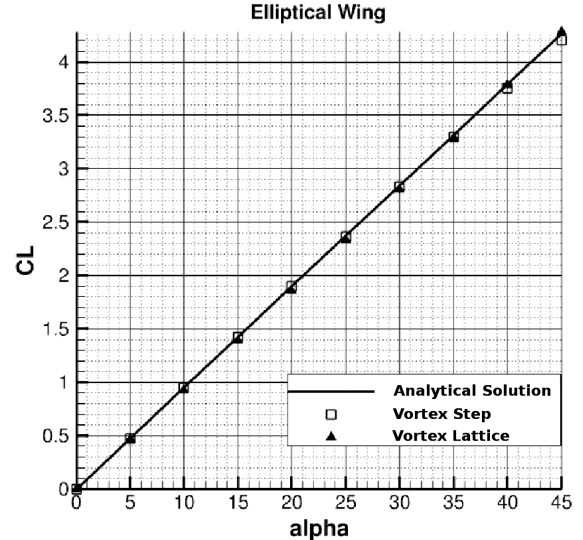


Fig. 1 Comparison of different potential flow implementations, elliptical wing, $\lambda = 12.7$.

3) Interpolate the sectional viscous lift at the effective angle of attack for each section:

$$\alpha_e = \alpha - \alpha_i \Rightarrow Cl_{vi}(\alpha_e) \quad (5)$$

4) Calculate the new circulation distribution using the Kutta–Joukowski theorem:

$$\Gamma = \frac{1}{2} V_\infty c Cl_{vi} \quad (6)$$

5) Update the new lift distribution for each station

$$\Gamma_{\text{input}} = \Gamma_{\text{old}} + d(\Gamma_{\text{new}} - \Gamma_{\text{old}}) \quad (7)$$

6) Repeat steps 2–5 until $|\Gamma_{\text{new}} - \Gamma_{\text{old}}| \leq \epsilon$ for each station, with ϵ being a user-selected convergence criteria.

The Γ method of Anderson [14] requires several hundred iterations with an underrelaxation factor of 0.05 to converge to machine accuracy and is unable to converge in the poststall region. Chattot [16] proposes a coupling algorithm based on a linearization of the Prandtl integrodifferential equation in dimensionless form, which is described next for completeness:

$$\Gamma(y) = \frac{1}{2} c(y) Cl[\alpha - \alpha_{0l}(y) + \arctan(w_{\text{ind}}(y))] \quad (8)$$

$$w_{\text{ind}}(y_n) = -\frac{1}{4\pi} \int_{-1}^1 \frac{\Gamma'(\eta)d\eta}{y_n - \eta} \quad (9)$$

$$\alpha_e = \alpha + \arctan(w_{\text{ind}}(y)) \quad (10)$$

The equation is discretized at position along the span, and integration points are placed between the nodes:

$$y_j = -\cos\left(\frac{j-1}{jx-1}\pi\right), \quad j = 1, \dots, jx \quad (11)$$

$$\eta_k = -\cos\left(\frac{k-1/2}{jx-1}\pi\right), \quad k = 1, \dots, jx-1 \quad (12)$$

Linearization with the Newton method is applied on the governing equation:

$$\Gamma_j + \Delta\Gamma_j = \frac{1}{2}c_j\left(Cl_j + \frac{dCl_j}{d\alpha}\Delta\alpha_e\right) \quad (13)$$

where

$$\Delta\alpha_e = \frac{\Delta w_{\text{ind}j}}{1+w_{\text{ind}j^2}}, \quad \Delta w_{\text{ind}j} = -\frac{1}{4\pi}\left(\frac{1}{y_j-\eta_{j-1}} - \frac{1}{y_j-\eta_j}\right)\Delta\Gamma_j = a_j\Delta\Gamma_j \quad (14)$$

The iterative equation takes the form

$$\left(1 - \frac{1}{2}c_j\frac{dCl_j}{d\alpha}\frac{a_j}{1+w_{\text{ind}j^2}}\right)\frac{\Delta\Gamma_j}{\omega} = \frac{1}{2}c_jCl_j - \Gamma_j^n \quad (15)$$

The equation is treated in increasing order of the j index. The circulation is updated as

$$\Gamma_j^{n+1} = \Gamma_j^n + \Delta\Gamma_j \quad (16)$$

Before stall ($\alpha \leq \alpha_{CL_{\max}}$), a unique solution can be found to Eq. (15), but poststall the nonlinearity leads to nonuniqueness of the solution. Chattot introduces artificial viscosity to the equation to couple the spanwise stations as well as to ensure the diagonal dominance of the left-hand-side matrix:

$$\begin{aligned} & \left(1 - \frac{1}{2}c_j\frac{dCl_j}{d\alpha}\frac{a_j}{1+w_{\text{ind}j^2}+2\mu}\right)\frac{\Delta\Gamma_j}{\omega} \\ &= \frac{1}{2}c_jCl_j - \Gamma_j^n + \mu(\Gamma_{j+1}^n - 2\Gamma_j^n + \Gamma_{j-1}^n) \end{aligned} \quad (17)$$

with

$$\mu \geq \max\left(\frac{1}{4}c_j\frac{dCl_j}{d\alpha}\frac{a_j}{1+w_{\text{ind}j^2}}, 0\right) \quad (18)$$

This method shows excellent results for poststall angles when the artificial viscosity is added, using a small underrelaxation factor. The comparison between the two algorithms is shown in Fig. 2 with analytical viscous data $Cl_{vi} = \pi \sin(2\alpha)$. The number of panels is set

to 200. Notice that the algorithm of Anderson presents a shift on this wing, and this will be further discussed in Sec. IV.C discussing the evaluation of the downwash angle. The theory of the elliptical wing indicates that the stall of the wing appears simultaneously on all sections of the wing, and Fig. 3 allows comparison of the lift distribution along the span close to stall for the numerical as well as the analytical solutions. The stall first appears close to the root and then propagates along the wing. This discrepancy with the theory can be attributed to the discretization errors of the numerical method, which, when combined to the nonlinear coupling procedures, lead to different stall propagation patterns. Indeed, these difficulties do not occur before the stall angle, where the coupling procedure leads to unique solutions.

B. α Methods

The α method of van Dam uses a modified Weissinger method as inviscid code, in which the position of the control point is adapted to reflect a slope equal to the viscous section slope Cl_{av} as follows.

1) Calculate the effective angle of attack for each section using the inviscid code

$$\alpha_e = \frac{Cl_{inv}}{Cl_{av}} + \alpha_{0l} - \Delta\alpha \quad (19)$$

2) Interpolate the sectional viscous lift at the effective angle of attack for each section:

$$\alpha_e = \alpha - \alpha_i \Rightarrow Cl_{vi}(\alpha_e) \quad (20)$$

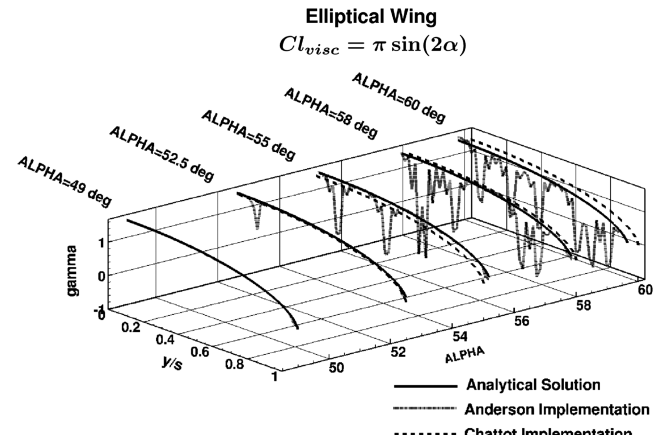


Fig. 3 Lift distribution near stall, elliptical wing, Anderson's algorithm.

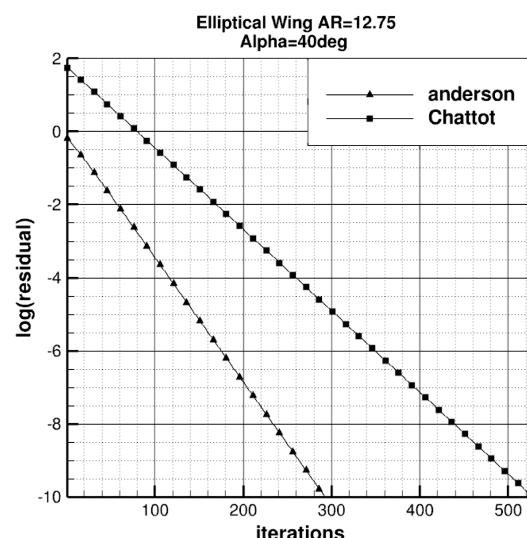
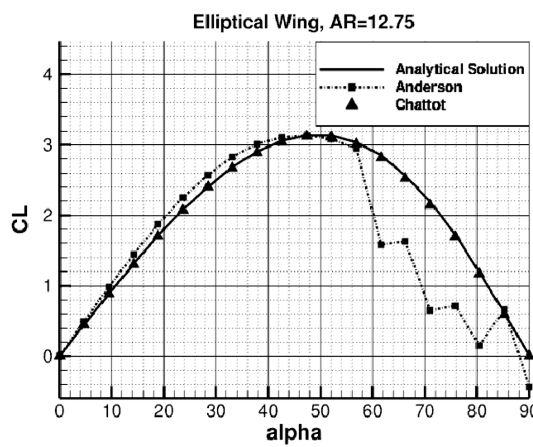


Fig. 2 Comparison between different Γ algorithms.

3) Calculate the angle of attack correction for each section:

$$\Delta\alpha = \frac{Cl_{vi} - Cl_{inv}}{Cl_{av}} \quad (21)$$

4) Update the angle of attack by the correction in the Weissinger method.

5) Repeat steps 1–4 until $|Cl_{vi} - Cl_{inv}| \leq \epsilon$.

This algorithm shows good results for analytical viscous data with a constant slope. However, the implementation of this method raises concerns when the slope becomes zero at the maximum lift angle, where Eq. (21) does not hold.

C. Effective Angle of Attack

We propose replacing the viscous slope Cl_{av} in Eqs. (19) and (21) by 2π , removing the dependency on the actual profile being used, while positioning the control point of the vortex step method to ensure that slope. This modification of the formulation proposed by van Dam to calculate the effective angle of attack can be understood with the help of Fig. 4.

If the viscous and inviscid lifts are equal,

$$Cl_{vi} = Cl_{inv} = 2\pi(\alpha - \Delta\alpha - \alpha_i) \quad (22)$$

then

$$\alpha - \alpha_i = \alpha_e = \frac{Cl_{inv}}{2\pi} + \Delta\alpha \quad (23)$$

To establish the sensitivity of Eq. (23) to different discretization schemes, three different ways to compute the effective angle of attack have been implemented and compared with analytical values for an elliptical wing.

The first implementation is performed using Prandtl's monoplane equation [17]. Representing the spanwise circulation distribution with a Fourier series,

$$\Gamma(\phi) = 2bV_\infty \sum_1^N A_N \sin(n\phi), \quad \frac{y}{b/2} = -\cos(\phi) \quad (24)$$

The coefficients A_N are calculated by solving the linear system of equations for a given $\Gamma(\phi)$ so that the induced angle of attack are calculated as

$$\alpha_i(\phi) = \frac{\sum nA_N \sin(n\phi)}{n \sin(\phi)} \quad (25)$$

The second implementation is the method proposed by Anderson [14], which is a numerical integration of the Eq. (4) using a midpoint

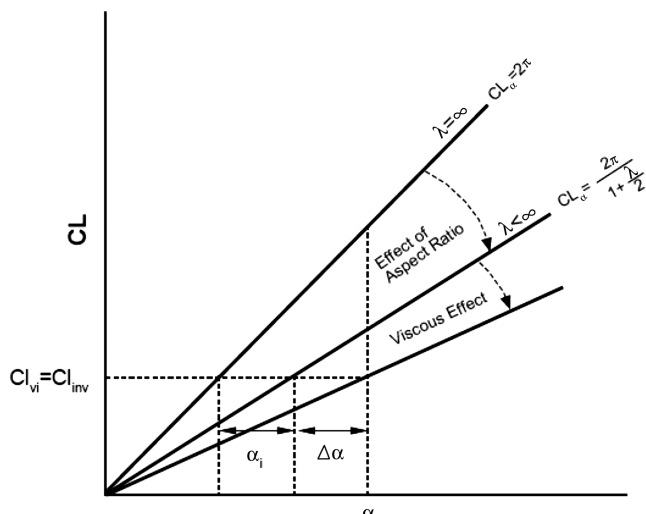


Fig. 4 Theoretical lift angle-of-attack curves, elliptical wing.

trapezoidal strategy, and the third implementation is our modified van Dam version of the effective angle of attack [Eq. (23)]. Note that this method does not require knowledge of $\Gamma(\phi)$, which for instance removes the need for the use of the Fourier series.

The effective angle of attack along the span for an elliptical wing is shown on Fig. 5, with 200 panels distributed along the span. All methods show discrepancies at the wing tip, due to the fact that the discontinuous induced velocity field at the wing tip is not appropriately captured by the discretized system.

A sensitivity study with respect to the number of panels used in the system is shown in Fig. 6, where values of the effective angle of attack at the wing root ($y/s = 0$) and wing tip ($y/s = 1$) are shown for an elliptical wing at $\alpha = 20$ deg. At the wing root, the three methods converge to a solution, with the van Dam implementation underestimating (0.5%), whereas other methods overestimate the value (2 and 3%). At the tip, only the van Dam implementation converges to a bounded solution, approaching the analytical value (0.5%). The integration scheme within Anderson's method give inaccurate results (150%), which explain the results obtained with this algorithm on the elliptical wing at high angle of attack observed in Fig. 2. In the reminder of the paper, we shall use this modified version of van Dam's approach.

D. Results

The α method with the modified van Dam's procedure presented in the previous section is used to provide results on linear and nonlinear viscous simulations over an elliptical wing of aspect ratio $\lambda = 12.75$. A comparison between van Dam's algorithm and our modification is presented in Fig. 7, on an analytical linear viscous data $Cl_{vi} = \eta 2\pi\alpha$. It can be observed that both algorithms present similar results.

The algorithm is then applied to an analytical viscous data $Cl_{vi} = \pi \sin(2\alpha)$. Figure 8 presents converged solutions in the poststall region that are not in agreement with the analytical behavior of the elliptical wing. Note that, if this implementation is replaced by its analytical value $\alpha_e = Cl/\pi\lambda$, the coupling algorithm is able to converge to the analytical solution (Fig. 8).

To estimate the robustness of the algorithm, tests have been conducted by adding a perturbation on the effective angle of attack at three different points along the span (10, 50, and 75% of the semispan). In the prestall region (Fig. 9), the perturbation is smoothed within the iterative scheme, making for a stable algorithm that provides the correct solution.

When approaching stall, a small perturbation can initiate the stall of the wing, as presented in Fig. 10. The perturbation propagates within the iterative scheme and shows different stall progressions depending on the initial point of application of the perturbation. There are right, left-and-right, and left propagation for the 10, 50, and

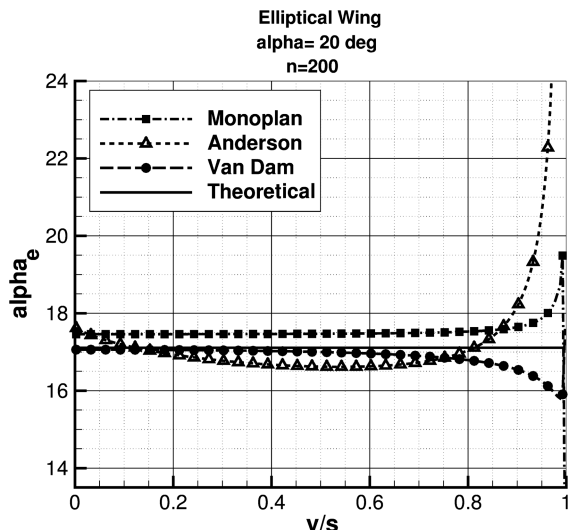


Fig. 5 Comparison of the effective angle of attack. Elliptical wing, $\alpha = 20$ deg.

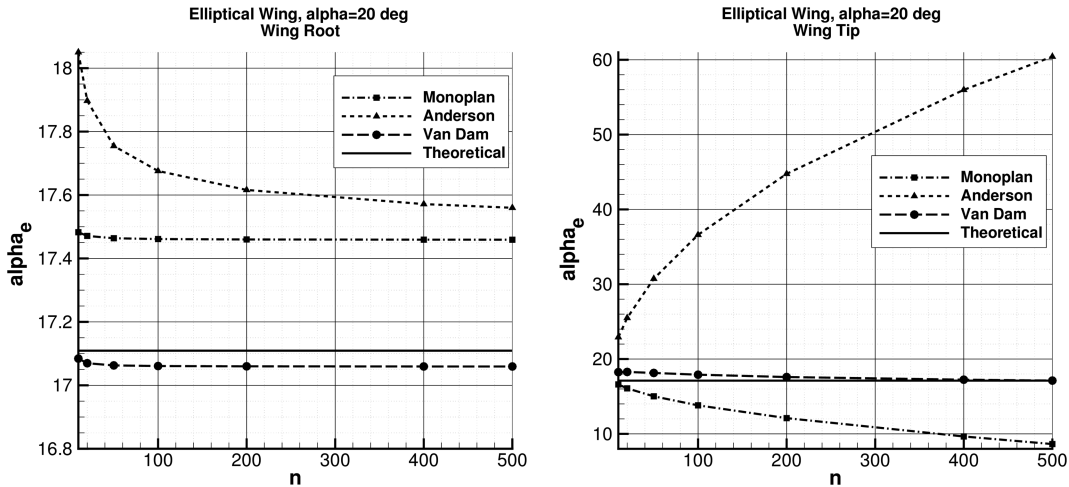


Fig. 6 Convergence of the induced angle of attack for various number of panels: wing root (left), wing tip (right).

75% disturbances, respectively. The different patterns show stall cells along the span, in agreement with the results observed by Weihs and Katz [18], Winkelmann and Barlow [19], and recently by Spalart [20].

Note that the algorithm still converges to machine zero for all simulations, albeit requiring more iterations. A method to accurately reproduce the analytical solution will be presented in Sec. V.C.

V. Strongly Coupled Algorithm

Borrowing from classical viscous–inviscid boundary-layer interaction developments in the 1970s, we present a strongly coupled algorithm. The differences between the loosely and strongly coupled algorithms are shown in Fig. 11. Linearizing the viscous correction and embedding the nonlinearity through an iterative procedure, one can write the resulting coupled set of linear equations in an expanded square matrix. For well-conditioned problems, convergence is reached in less iterations for the strongly coupled scheme.

A. Elliptical Wing, Analytical Formulation

The procedure is applied to the elliptical wing problem of Sec. IV, where the analytical viscous section lift coefficient is given by $Cl_{vi} = \pi \sin(2\alpha)$.

For the inviscid part, the lift can be written as

$$Cl_{inv} = \frac{2\pi(\alpha - \Delta\alpha)}{1 + 2/\lambda} \quad (26)$$

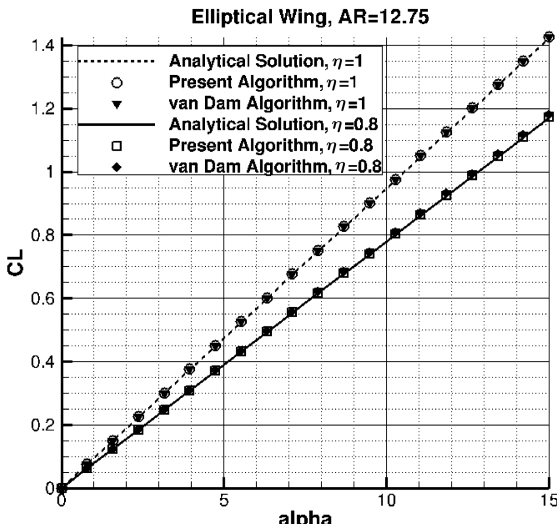


Fig. 7 Elliptical wing with analytical lift.

The effective angle of attack is then

$$\alpha_e = \frac{\alpha - \Delta\alpha}{1 + 2/\lambda} + \Delta\alpha \quad (27)$$

Placing the unknowns on the left-hand side, we obtain

$$\alpha_e - \left(1 - \frac{1}{1 + 2/\lambda}\right)\Delta\alpha = \frac{\alpha}{1 + 2/\lambda} \quad (28)$$

The viscous correction is calculated with the following equation:

$$\Delta\alpha = \frac{2\pi\alpha_e - \pi \sin(2\alpha_e)}{2\pi} \quad (29)$$

A first-order Taylor series expansion is applied to linearize the section viscous lift data:

$$\sin(2\alpha_e^{n+1}) = \sin(2\alpha_e^n) + 2 \cos(2\alpha_e^n)(\alpha_e^{n+1} - \alpha_e^n) \quad (30)$$

Again, placing the unknowns on the left-hand side, we obtain

$$(1 - \cos(2\alpha_e^{n+1}))\alpha_e^{n+1} - \Delta\alpha = \frac{1}{2} \sin(2\alpha_e^n) - \alpha_e^n \cos(2\alpha_e^n) \quad (31)$$

The inviscid and viscous equations can be assembled in a matrix and solved with a classic inversion method:

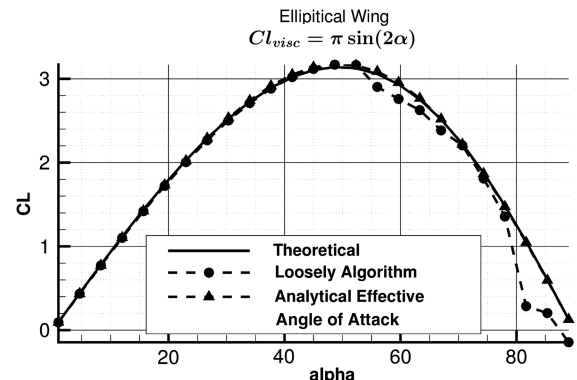


Fig. 8 Loosely coupling algorithm, comparison with analytical effective angle of attack α_e .

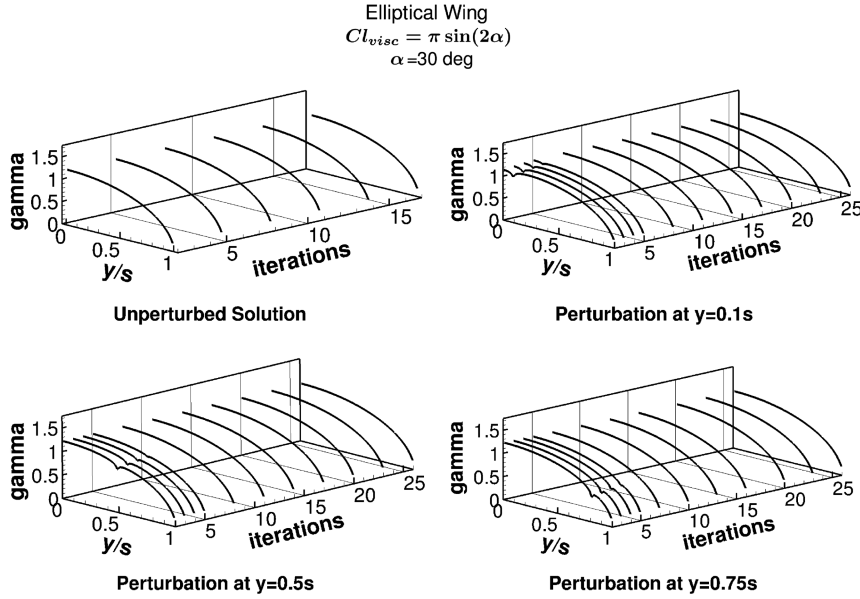


Fig. 9 Elliptical wing, perturbation of the effective angle of attack in the linear region.

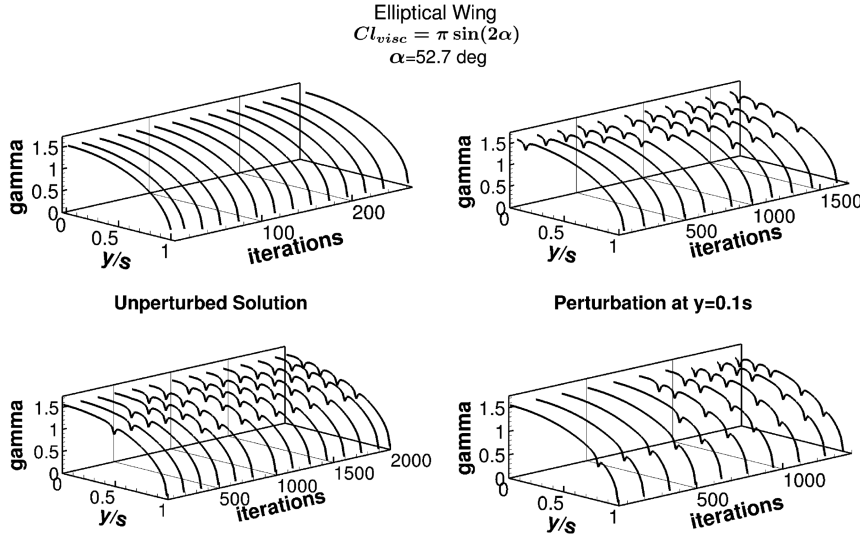


Fig. 10 Elliptical wing, perturbation of the effective angle of attack close to the stall.

$$\begin{bmatrix} 1 & \left(\frac{1}{1+2/\lambda} - 1\right) \\ 1 - \cos(2\alpha_e^n) & -1 \end{bmatrix} \begin{bmatrix} \alpha_e^{n+1} \\ \Delta\alpha^{n+1} \end{bmatrix} = \begin{bmatrix} \frac{\alpha}{1+2/\lambda} \\ \frac{1}{2} \sin(2\alpha_e^n) - \alpha_e^n \cos(2\alpha_e^n) \end{bmatrix} \quad (32)$$

The improved convergence curve is represented in Fig. 12, where the strongly coupled procedure reaches machine zero in five iterations, compared to 16, 400, and 650 iterations with the loosely coupled α method, Chattot's method, and Anderson's Γ method, respectively.

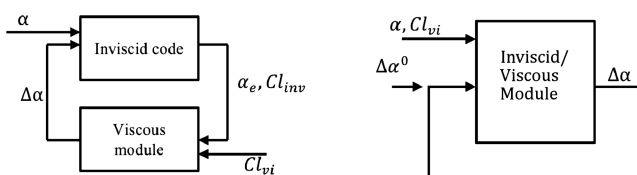


Fig. 11 Representation of the coupling algorithm: loosely coupled (left), strongly coupled (right).

B. General Wing, Discrete Formulation

We present two numerical implementations based on the modified van Dam algorithm. The two linear sets of equations are the vortex lattice method equations and the viscous correction:

$$\begin{bmatrix} I_{11}\Gamma_1 + I_{12}\Gamma_2 + \dots + I_{1n}\Gamma_n \\ \vdots \\ I_{n1}\Gamma_1 + I_{n2}\Gamma_2 + \dots + I_{nn}\Gamma_n \end{bmatrix} = \begin{bmatrix} \sin(\alpha - \Delta\alpha_1) \\ \vdots \\ \sin(\alpha - \Delta\alpha_n) \end{bmatrix} \quad (33)$$

$$\begin{bmatrix} \Delta\alpha_1 \\ \vdots \\ \Delta\alpha_n \end{bmatrix} = \begin{bmatrix} \frac{Cl_{vi1}-Cl_{mv1}}{2\pi} \\ \vdots \\ \frac{Cl_{vin}-Cl_{mvn}}{2\pi} \end{bmatrix} = \begin{bmatrix} \frac{Cl_{vi1}-2\Gamma_1/c_1 V_\infty}{2\pi} \\ \vdots \\ \frac{Cl_{vin}-2\Gamma_n/c_n V_\infty}{2\pi} \end{bmatrix} \quad (34)$$

The variables of the system are the lift circulation $[\Gamma_1, \dots, \Gamma_n]$ and the viscous correction $[\Delta\alpha_1, \dots, \Delta\alpha_n]$. A standard reduced Newton-Raphson method is used to solve this extended nonlinear system of equation:

$$X_{n+1} = X_n - [F'(X_n)]^{-1} F(X_n) = X_n - J^{-1}(X_n) F(X_n) \quad (35)$$

where $X_n = [\Gamma_1, \dots, \Gamma_n, \Delta\alpha_1, \dots, \Delta\alpha_n]$ is the vector of variables, and $F(X_n)$ and $J(X_n)$ are the vector of function values and the Jacobian, respectively.

The method needs to interpolate the viscous section lift coefficient, requiring the induced angles of attack. Two loops are then necessary, with the first solving the nonlinear system of equation and the second interpolating the viscous lift to update the nonlinear system. Tests have been conducted and show that only one iteration of the Newton–Raphson method is sufficient. Note that, during one iteration, the interpolated viscous lift coefficient is considered as a constant, and its derivatives with respect to the system variables are equal to zero. As expected, the coupling algorithm converges to the same solution as the one obtained from resolving the nonlinear system with multiple iterations.

To construct a strongly coupled algorithm for the general case of any lift curve, numerical series of the viscous lift session is constructed. Legendre series using Gauss–Legendre quadrature is used to properly represent the curves:

$$Cl_{vi}(\alpha_e) = \sum_{k=0}^N w_k P_k(\alpha_e) \quad (36)$$

with

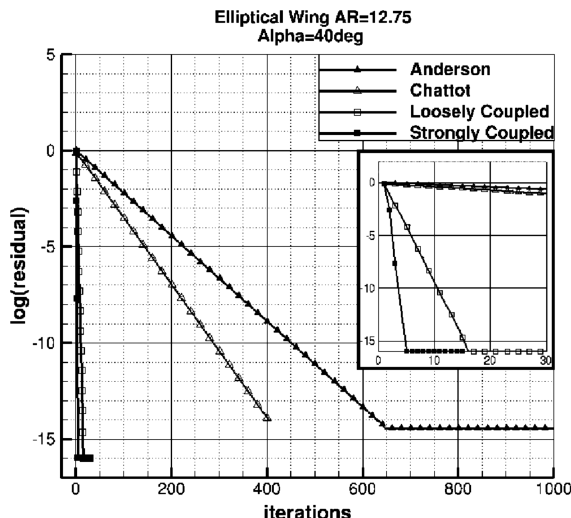


Fig. 12 Convergence of analytical coupling.

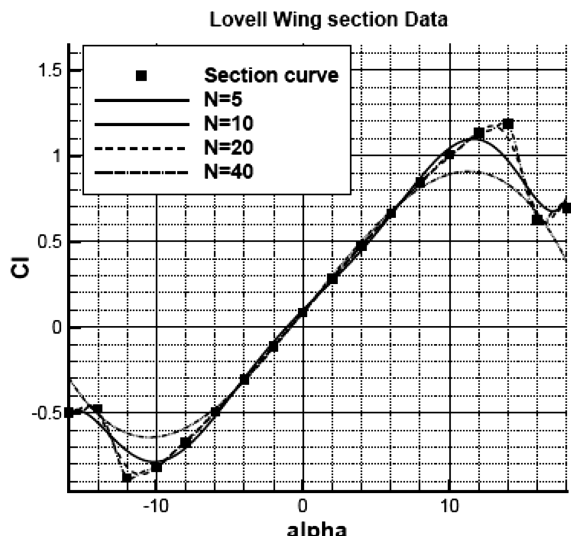


Fig. 13 Influence of the number of terms in the Legendre series.

Table 1 Legendre polynomials interpolation error ($\alpha = 12$ deg)

| Number of terms | Error, % |
|-----------------|----------|
| 5 | 20.3 |
| 10 | 3.45 |
| 20 | 0.48 |
| 40 | 0.02 |

$$w_k = \frac{2}{(1-x_i)^2[P'(x_i)]^2} \quad (37)$$

x_i are the Gauss interpolation points, and $P(x_i)$ and $P'(x_i)$ are the Legendre polynomials and derivatives. The right-hand side of Eq. (34), using our definition of the effective angle of attack $\alpha_e = (Cl_{inv}/2\pi) - \Delta\alpha$, becomes

$$\begin{bmatrix} \frac{Cl_{vi1}-2\Gamma_1/c_1 V_\infty}{2\pi} \\ \vdots \\ \frac{Cl_{vin}-2\Gamma_n/c_n V_\infty}{2\pi} \end{bmatrix} = \begin{bmatrix} \sum_{k=0}^N w_k P_k(\Gamma_1/\pi V_\infty c_1 - \Delta\alpha_1) \\ \vdots \\ \sum_{k=0}^N w_k P_k(\Gamma_n/\pi V_\infty c_n - \Delta\alpha_n) \end{bmatrix} \quad (38)$$

This algorithm bypasses the need for interpolation. Newton–Raphson iterations are used to solve the nonlinear system only once.

Figure 13 shows the approximation of the lift curve using different number of points. Table 1 present the relative interpolation error at an angle of 12 deg. It can be inferred that 40 terms are adequate, and this is the number used in the rest of the study.

Three cases are used to compare the convergence behavior of the three implementations of the coupling algorithm: the loosely coupled, the strongly coupled with interpolation, and the “fully strongly” coupled algorithm, using the Legendre series of the viscous lift curves.

Results on elliptical wing with the analytical viscous section lift $Cl_{vi} = \pi \sin(2\alpha)$ already studied are represented in Fig. 14. Residual convergences are presented in Fig. 15. The three implementations show similar results in the linear region. In the poststall region, the three algorithms converge but to different results, as expected from the analysis of the previous section. Figure 16 shows results similar to Fig. 3, the stall progression for the loosely coupled implementation. The stall initiates close to the root and propagates along the span. The stall cells are clearly visible and present the same pattern as those presented in Fig. 10.

The results obtained with the strongly coupled algorithms are not represented in the figure because they present the same behavior as the loosely coupled version. For these α method algorithms, the lift circulation is smoother along the span than the Γ method algorithm implemented by Anderson, but the propagation of the stall is similar. As mentioned previously, a modification to ensure compatibility of the numerical solution to the analytical result is presented in the next section.

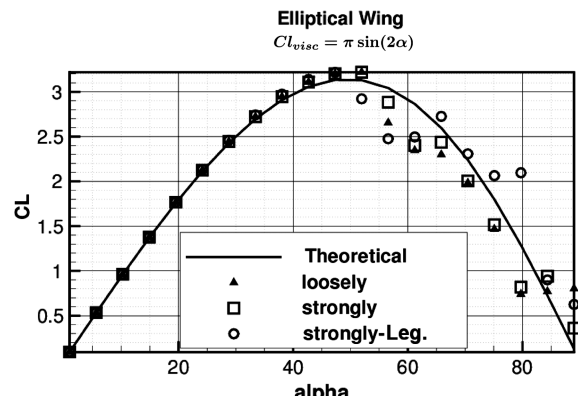


Fig. 14 Elliptical wing, comparison of strongly and loosely implementations.

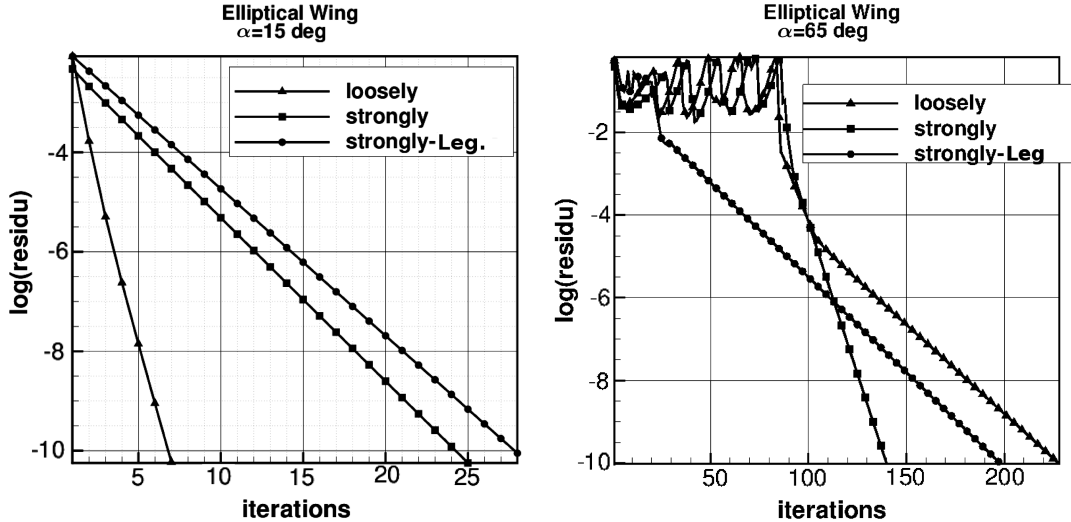


Fig. 15 Elliptical wing, convergence for a prestall and a poststall angle of attack.

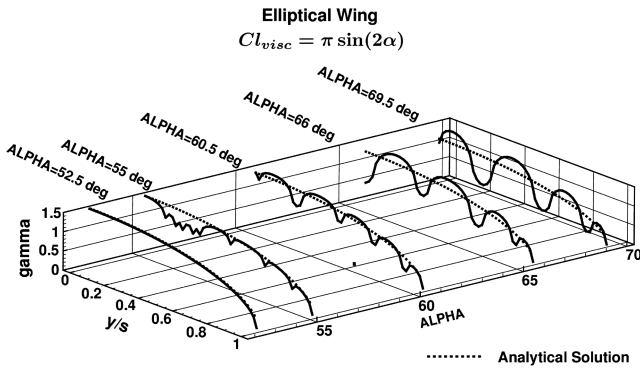


Fig. 16 Lift distribution near stall, elliptical wing, loosely coupled algorithm.

C. Artificial Viscosity

Based on the work of Chattot [16], which introduced artificial viscosity within the Γ method, artificial viscosity has been added to the viscous correction of the α method:

$$F_i(\Gamma, \Delta\alpha) = \Delta\alpha_i - \frac{Cl_{vi}}{2\pi} + \frac{\Gamma_i}{\pi V_\infty c_i} - \mu_i(\Delta\alpha_{i-1} - 2\Delta\alpha_i + \Delta\alpha_{i+1}) \quad (39)$$

This term has been implemented in the strongly coupling algorithm using the Legendre series. The value of the artificial viscosity coefficient has been chosen to ensure that the diagonal term of the

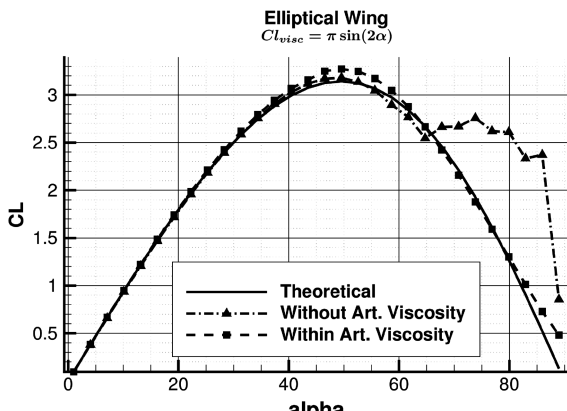


Fig. 17 Elliptical wing, lift coefficient within artificial viscosity.

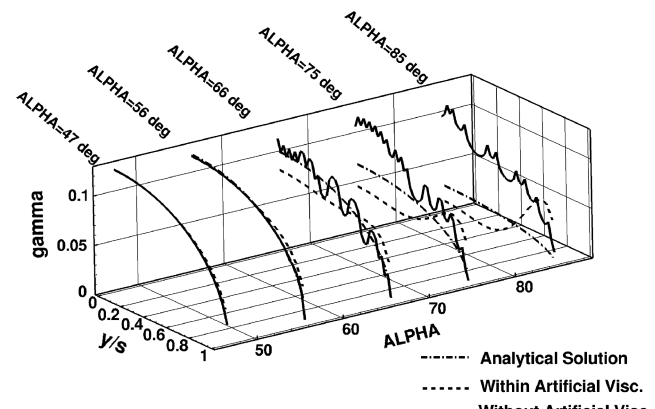


Fig. 18 Elliptical wing, lift distribution near stall within artificial viscosity.

Jacobian matrix, the derivative of the equation with respect to the viscous correction, is larger than the derivative of the equation with respect to the lift distribution:

$$\begin{aligned} \frac{\partial F_i}{\partial \Delta\alpha_i} &\geq \frac{\partial F_i}{\partial \Gamma_i} \Rightarrow \mu_i \\ &\geq \max \left(0, -\frac{1}{2} \left[\frac{1}{2\pi} \sum_{k=0}^N w_k P'_k \cdot \left(\frac{1}{\pi V_\infty c_i} + 1 \right) - \left(\frac{1}{\pi V_\infty c_i} - 1 \right) \right] \right) \end{aligned} \quad (40)$$

The effects of the artificial viscosity are presented in Figs. 17 and 18, on the elliptical wing with the analytical viscous lift $Cl = \pi \sin(2\alpha)$. The solution now converges to a solution closer to the analytical value. The differences, which are clearly visible past 60 deg, are due to the addition of the artificial viscosity term to the right-hand side of the system, thus affecting the solution.

As expected, the lift distribution with the artificial viscosity term is smoother than the solution without artificial viscosity.

VI. Conclusions

Different coupling algorithms have been implemented and compared. The Γ methods require an important underrelaxation factor to converge, and artificial viscosity has to be implemented to converge in the poststall region. The α methods converge faster than Γ methods, without relaxation, and are better suited to capture near-stall effects. An efficient α method algorithm has been devised that presents excellent results and fast convergence, even at high angle of

attack, and is able to predict the pre/poststall lift coefficients with accuracy suitable in a preliminary design framework.

The loosely coupled algorithm has been used on an elliptical wing using four different estimations of the effective angle of attack. The analytical estimation matches the analytical behavior of the elliptical wing, but the others methods converge to different solutions in the poststall region. The instabilities of the algorithms have been highlighted by using different initial perturbations of the effective angle of attack, leading to different solutions in the poststall region.

A new strongly coupled algorithm has been implemented for the analytical case and is shown to provide machine-accurate convergence in five nonlinear iterations on the elliptical wing. Two numerical implementations of the strongly procedure have been implemented, one requiring interpolation in the section viscous data, and the second version using Legendre series of the viscous section data, removing the need for interpolation. Artificial viscosity has been added to the strongly coupling algorithm using the α method and allows recovery of the analytical solution in the poststall region, with minor changes to the solution.

Acknowledgments

The work has been performed through a collaborative research and development grant 429243-11 with Bombardier Aerospace, the Consortium de Recherche et d’Innovation en Aérospatiale au Québec, and the Natural Sciences and Engineering Research Council of Canada. The authors thank Marcin Chrust for his help with the Legendre polynomials implementation.

References

- [1] Valarezo, W. O., and Chin, V. D., “Maximum Lift Prediction for Multielement Wings,” *30th Aerospace Sciences Meeting and Exhibit*, AIAA Paper 1992-0401, Jan. 1992.
- [2] Cebeci, T., Shao, J., Kafyeke, F., and Laurendeau, E., *Computational Fluid Dynamics for Engineers: From Panel to Navier–Stokes Methods with Computer Programs*, Springer, New York, 2005, pp. 10–17.
- [3] Hess, J. L., and Smith, A., “Calculation of Non-Lifting Potential Flow About Arbitrary Three-Dimensional Bodies,” Defense Technical Information Center TR, ES-40622, Fort Belvoir, VA, 1962.
- [4] Phillips, W., and Alley, N., “Predicting Maximum Lift Coefficient for Twisted Wings Using Lifting-Line Theory,” *Journal of Aircraft*, Vol. 44, No. 3, 2007, pp. 898–910.
doi:10.2514/1.25640
- [5] Weissinger, J., “The Lift Distribution of Swept-Back Wings,” NACA TR-1120, 1947.
- [6] Blackwell, J., “A Finite-Step Method for Calculation of Theoretical Load Distributions for Arbitrary Lifting-Surface Arrangements at Subsonic Speeds,” NASA TR, 1969.
- [7] Tani, I., “A Simple Method of Calculating the Induced Velocity of a Monoplane Wing,” Aeronautical Research Inst., Tokyo Imperial Univ., Rept., Vol. 111, 1934.
- [8] Sivells, J., and Neely, R., “Method for Calculating Wing Characteristics by Lifting-Line Theory Using Nonlinear Section Lift Data,” NACA TR-1269, 1947.
- [9] Piszkin, S., and Levinsky, E., “Nonlinear Lifting Line Theory for Predicting Stalling Instabilities on Wings of Moderate Aspect Ratio,” General Dynamics, Convair Division, TR, CASD-NSC-76-001, San Diego, CA, 1976.
- [10] Wickheiser, A. M., and Garcia, E., “Extended Nonlinear Lifting-Line Method for Aerodynamic Modeling of Reconfigurable Aircraft,” *Journal of Aircraft*, Vol. 48, No. 5, 2011, pp. 1812–1817.
doi:10.2514/1.C031406
- [11] Mukherjee, R., Gopalarathnam, A., and Kim, S. W., “An Iterative Decambering Approach for Post-Stall Prediction of Wing Characteristics from Known Section Data,” *41st Aerospace Sciences Meeting and Exhibit*, AIAA Paper 2003-1097, Jan. 2003.
- [12] Tseng, J., and Lan, C., “Calculation of Aerodynamic Characteristics of Airplane Configurations at High Angles of Attack,” NASA TR 4182, 1988.
- [13] Van Dam, C., “The Aerodynamic Design of Multi-Element High-Lift Systems for Transport Airplanes,” *Progress in Aerospace Sciences*, Vol. 38, No. 2, 2002, pp. 101–144.
doi:10.1016/S0376-0421(02)00002-7
- [14] Anderson, J., *Fundamentals of Aerodynamics*, Vol. 2, McGraw–Hill, New York, 2001, pp. 387–390.
- [15] Katz, J., and Plotkin, A., *Low-Speed Aerodynamics*, Vol. 13, Cambridge Univ. Press, Cambridge, England, U.K., 2001, pp. 546–601.
- [16] Chattot, J.-J., “Analysis and Design of Wings and Wing/Winglet Combinations at Low Speeds,” *Computational Fluid Dynamic Journal*, Vol. 13, No. 3, Oct. 2004, pp. 1–99.
- [17] Bertin, J., *Aerodynamics for Engineers*, Prentice–Hall, Englewood Cliffs, NJ, 2002, pp. 333–338.
- [18] Weihl, D., and Katz, J., “Cellular Patterns in Poststall Flow over Unswept Wings,” *AIAA Journal*, Vol. 21, No. 12, 1983, pp. 1757–1759.
doi:10.2514/3.8321
- [19] Winkelman, A. E., and Barlow, J. B., “Flowfield Model for a Rectangular Planform Wing Beyond Stall,” *AIAA Journal*, Vol. 18, No. 8, 1980, pp. 1006–1008.
doi:10.2514/3.50846
- [20] Spalart, Philippe R., “Prediction of Lift Cells for Stalling Wings by Lifting-Line Theory” *AIAA Journal*, Vol. 52, No. 8, pp. 1817–1821.

G. Blaisdell
Associate Editor